Micromagnetic modelling of stripe domains in thin films with a columnar microstructure

Cite as: AIP Advances **11**, 015319 (2021); https://doi.org/10.1063/9.0000206
Submitted: 25 October 2020 . Accepted: 04 December 2020 . Published Online: 07 January 2021

E. Yu. Dengina, A. S. Bolyachkin, N. A. Kulesh, and V. O. Vas'kovskiy

Micromagnetic modelling of stripe domains in thin films with a columnar microstructure

Cite as: AIP Advances 11, 015319 (2021); doi: 10.1063/9.0000206
Presented: 6 November 2020 • Submitted: 25 October 2020 •
Accepted: 4 December 2020 • Published Online: 7 January 2021

E. Yu. Dengina,[1,a)] A. S. Bolyachkin,[1] N. A. Kulesh,[1] and V. O. Vas'kovskiy[1,2]

AFFILIATIONS

[1] Ural Federal University, 19 Mira St., 620002 Yekaterinburg, Russia
[2] Institute of Metal Physics UB RAS, 18 S. Kovalevskaya St., 620108 Yekaterinburg, Russia

Note: This paper was presented at the 65th Annual Conference on Magnetism and Magnetic Materials.
[a)] **Author to whom correspondence should be addressed:** dengina.ekaterina@urfu.ru

ABSTRACT

A micromagnetic model of thin films with columnar microstructure in the form of a matrix with reduced magnetic properties and embedded columns with high aspect ratio is presented. Such microstructure is typical for some films based on rare-earth and 3d transition metal alloys, in particular for La-Co films, that were chosen as an object for our modelling. Described structural features promote an effective perpendicular magnetic anisotropy that for thick enough films leads to formation of the stripe domain pattern. Our work addresses to the problem of finding equilibrium characteristics of stripe domains for the case of infinite columnar films. Herein it is shown how width of stripe domains, remanent magnetization and energies depend on number of replicas of periodic boundary conditions and the size of modelling volume. Equilibrium values of listed quantities can be found by extrapolating obtained dependencies.

I. INTRODUCTION

A long history of studying thin magnetic films yielded a great variety of magnetic patterns such as vortices, periodic stripes, disordered labyrinth domains, etc. having domain walls of different types and a diversity of topological defects.[1] The importance of thin films for applications in spintronics and magnetic storage of information specifies a necessity of deep understanding how microstructural features and micromagnetic properties of films as well as external conditions determine their domain structure and how it can be tuned. Let us consider this problem further for a certain case of domain structure – a stripe domain pattern.

The stripe domain pattern is characterized by periodic out-of-plane magnetization oscillations.[2] It appears above a critical film thickness D_{cr} and it is usually induced by the magnetic anisotropy with out-of-plane easy magnetization axis that joins the competition between short-range exchange and long-range magnetostatic interactions. For small magnetic anisotropy (quality factor $Q < 1$) magnetization oscillates in a flux-closed manner (weak stripe domains), while for large anisotropy the oscillation mode is one-dimensional (strong stripe domains).[2] One of the earliest theoretical description of strong stripe domains in uniform films was done by Kittel[3] assuming the square magnetization profile. This approximation is valid only when the film thickness D is much larger than domain width W and the last one is much larger than the width of domain walls δ ($\delta \ll W \ll D$). The Kittel model allowed to demonstrate the magnetization transition from in-plane to out-of-plane direction at D_{cr} and to find the dependence $W \sim \sqrt{D}$. The case of weak stripe domains can be described in a similar way using the sawtooth magnetization model.[4] Further development of the Kittel approach for uniform films was done recently in Ref. 5, where asymptotic behavior of the width of stripe domains close to the critical field was considered and in Refs. 6 and 7 where sinewave wall model was used with more accurate accounting for magnetostatic interactions and with explicitly treated domain walls. The micromagnetic solution of the nucleation problem for stripe domains was proposed by Muller.[8] In particular he found analytical expression for the critical thickness $D_{cr} = \left(2\pi\sqrt{A/K}\right)/(1-h)$ and corresponding domain width $W_{cr} = D_{cr}\sqrt{(1-h)/(1+h)}$ for the limiting case of $Q \ll 1$. Here A is an exchange constant, K is an anisotropy constant and h is an external magnetic field H normalized on the anisotropy field, i.e., $h = HM_s/(2K)$, where M_s is

a saturation magnetization. Starting from the pioneering work of Muller,[8] numeric micromagnetic approach and especially computer modelling became one of the main instruments for analyzing stripe domain patterns.[9–16]

Not only uniform magnetic films are of current research interest,[16–18] a great attention is focused on the analysis of stripe domains in films having nonuniformities of different kinds. First multilayered magnetic films can be mentioned.[12,19,20] For them an intriguing opportunity of the evaluation of interfacial Dzyaloshinskii–Moriya interaction from the parameters of stripe domains was reported.[19,20] Influence of a lattice of artificial defects in the form of antidot or honeycomb on stripe domains was also studied and some features of topological defects were revealed.[14] The next example of a nonuniform film is one with a gradient of perpendicular magnetic anisotropy constant with the thickness that resulted in the asymmetry of stripe domains.[13] Finally, lets us focus on amorphous thin films of alloys of rare-earth (R) and 3d transition metals (TM). In such films both perpendicular magnetic anisotropy and stripe domain pattern are observed frequently. There could be different origins of the anisotropy: the anisotropic distribution of nearest-neighbor R-T pairs formed during the film deposition (pseudocrystalline model), spin–orbit coupling resulting in single-ion anisotropy or anisotropic exchange, stress-induced anisotropy.[21,22] Depending on the type of R ion and sputtering conditions, different mechanisms can prevail. Another possibility for anisotropy formation is related to a columnar microstructure of R-TM films, which was revealed in Refs. 23 and 24. This nonuniformity can lead to structure-induced effective perpendicular magnetic anisotropy, which can be quantified using parameters of stripe pattern.

In this work thin magnetic films with columnar microstructure were studied using micromagnetic modelling. It is demonstrated further that such nonuniform structure can lead itself to stripe domains without any explicit perpendicular magnetic anisotropy. The aim of the work was to estimate equilibrium width of stripe domains corresponding to the infinite columnar film. For that the effects of modelling volume size and periodic boundary conditions were analyzed systematically for the case of a film with realistic micromagnetic parameters taken for La-Co alloy.

II. DETAILS OF COMPUTER SIMULATIONS

Amorphous La-Co films with a columnar microstructure were chosen as an object for a computer model, which was created in two stages. At the first stage, the columnar microstructure was constructed using the MATLAB software package. At the beginning of this process a two-dimensional grid of points with a hexagonal ordering was generated (Fig. 1a, blue crosses). The distances between the points were chosen so that the final average size of the columns, calculated as $\sqrt{S}$, where S is a cross-sectional area of the columns, was of a desired value. To simulate irregular shapes of columns, the points were shifted along the plane by random vectors, which components were set by the normal distribution with zero mean and a certain variance (Fig. 1a, black dots). A standard deviation σ of column sizes was tuned by choosing the appropriate variance of random shifts. In our calculations value of σ normalized on the mean $\sqrt{S}$ was of 0.1. To avoid edge effects, as well as to simulate infinite films, periodic boundary conditions were created: several rows of edge-points were duplicated toward the opposite sides of the modelling area (Fig. 1a, red points). Then 2D Voronoi tessellation was applied to all points (Fig. 1a, dashed lines). After that, a homothety with respect to the centroids of polyhedra was carried out in order to create a matrix between columns. In this way one layer of the film was formed and then was translated over the entire thickness of the film. The scaled image of the final columnar microstructure is shown in the Figure 1b.

At the second stage the geometry with columnar microstructure was loaded into the Mumax3 program[25] for micromagnetic simulations. Discretization size was set at 1 nm so that columns with typical size of about 5 nm remained sufficiently resolvable. The following energy contributions were considered: Magnetostatic energy, exchange interaction energy, and Zeeman energy. Equilibrium magnetization configuration at remanence was of interest and was calculated in the energy minimization mode (minimize() function) starting from the magnetic saturation and gradually reducing external magnetic field. Thus, a zero-temperature approximation was used. Size of the modelling area was varied from 120 to 500 nm with fixed thickness of 50 nm. The choice of these sizes was due to a compromise – the modelling area should be large enough to form stripes, but the computation time should remain acceptable within the available computing resources. Periodic boundary conditions (PBC) within the plane were taken into account with the number of replicas varying from 3 to 36.

For our modelling we assumed that in LaCo films the content of La in columns is on Δx less than in surrounding matrix. Thus, for the nominal composition of La_xCo_{1-x}, compositions of columns and the matrix are $La_{x-(1-s)\Delta x}Co_{1-x+s\Delta x}$ and $La_{x+s\Delta x}Co_{1-x-(1-s)\Delta x}$ respectively, where s is the volume ratio of these phases. In this work s was chosen to be 0.5. Since magnetic properties of the R-Co systems strongly depend on the composition, for micromagnetic

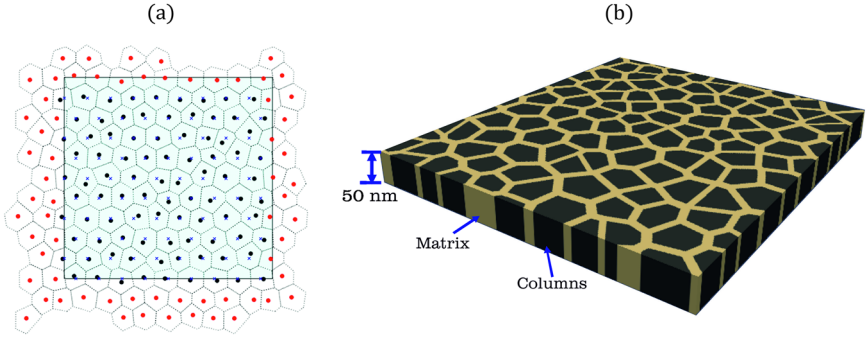

FIG. 1. (a) Generation of a grid of points with hexagonal ordering (blue crosses) and their random shifts (black points). Red points provide periodic boundary conditions. Dashed lines indicate Voronoi polyhedra constructed for the points. The target area for simulations is shown in a blue rectangle. (b) Final computer model of a thin film with the columnar microstructure.

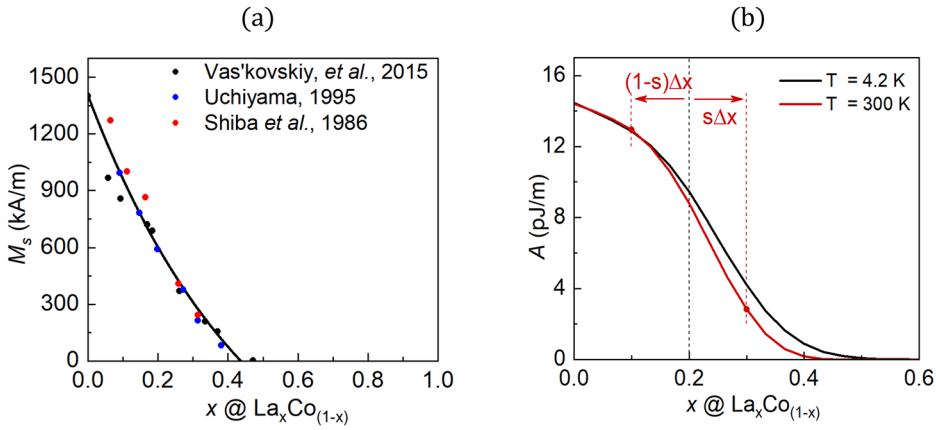

FIG. 2. Concentration dependencies of saturation magnetization (a) and exchange constant (b) for amorphous alloys LaCo.

simulations of two-phase LaCo films different values of saturation magnetization and exchange constant were specified for columns and the matrix relying on experimental data. Figure 2a shows the concentration dependence of $M_s(x)$ for LaCo at room temperature obtained from Refs. 26–28. A good agreement between the data can be seen, therefore $M_s(x)$ was interpolated over the entire set of points (Fig. 2a; solid line). Similar dependences for the exchange constant $A(x)$ are not presented in the literature. So, they were reproduced using the environment model, which was originally developed to describe the $M_s(x)$ of amorphous alloys of rear earth and 3d-metals.[29] Applied to La_xCo_{1-x}, it is assumed that all Co atoms have a number of neighbors $n = 12$, among which with the probability $P(x,n,k) = C_n^k \cdot x^k(1-x)^{n-k}$ there can be k nonmagnetic La atoms, where $C_n^k = n!/[k!(n-k)!]$. The next assumption is that a threshold number t of La atoms among neighbors is introduced for Co atoms. For $k > t$, the Co atom does not carry a magnetic moment, and for $k \le t$ it has a spin magnetic moment μ_s. In a simplified form, this reflects the effect of charge transfer in the framework of the band theory. Then the dependence $\mu(x)$ can be described by the following expression:

$$\mu(x) = \mu_s \sum_{k=0}^{t} P(x,n,k). \quad (1)$$

This statistical approach can be similarly used to calculate $A(x)$:

$$A(x) = \frac{\sqrt{2}J}{6a} \sum_{k=0}^{t} P(x,n,k) \cdot (n-k)\mu^2(x), \quad (2)$$

where $J = 2.1 \cdot 10^{-21}$ J is the energy of the exchange interaction between Co atoms, $a = 0.25$ nm is the distance between them, k_b is the Boltzmann constant, $t = 4$ and $\mu_s = 0.78$, taken from Refs. 26 and 30 Expression (2) gives the dependence shown in Figure 2b. It should be noted that with these constants, the dependence $A(x)$ is valid at low temperatures, i.e., $T = 4.2$ K, and it can be corrected for room temperature in a common way: $A(x,T) = A(x,0) \cdot [M_s(x,T)/M_s(x,0)]^{1.8}$[30]. For this, the ratios $M_s(x,T)/M_s(x,0)$ at different x were extracted from the experimental data[26] and interpolated. The corrected dependence $A(x)$ (Fig. 2b; red line) takes zero value at $x_c \approx 0.45$ that is consistent with the critical concentration for $M_s(x)$ (Fig. 2a), in addition, $A(0) = 14.4$ pJ/m that correlates with the exchange constant for Co.[30]

The nominal composition $La_{0.2}Co_{0.8}$ was chosen for computer simulations. The difference in the La content between the columns and the matrix was taken as $\Delta x = 0.3$. At smaller Δx for the selected geometric parameters, it was not possible to observe the formation of stripes. Thus, for the columns, the saturation magnetization and the exchange constant were 1160 kA/m and 14 pJ/m. For the matrix separating the columns, they were respectively equal to 180 kA/m and 1 pJ/m.

III. RESULTS AND DISCUSSION

Micromagnetic modelling of columnar LaCo films was performed for a series of lateral sizes L from 120 nm to 500 nm with fixed thickness of 50 nm and columns size of 5 nm along with its reduced standard deviation of 0.1. A square shape of films was chosen mostly for cases with $L < 200$ nm, while for larger films the side along stripes was shorten twice to reduce the time of calculations. To compensate this reduction, a number of PBC replicas along this dimension was proportionally increased. However, let us note that

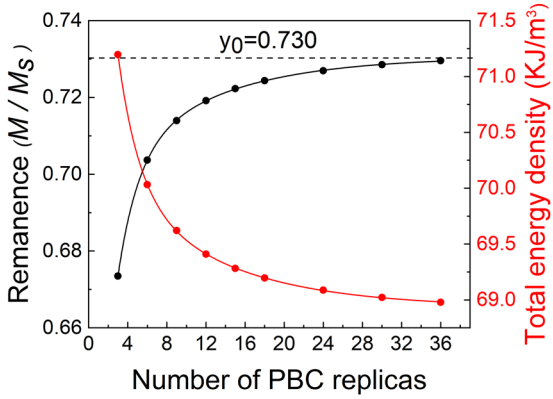

FIG. 3. Dependencies of reduced remanence and total energy density of the LaCo columnar film on number of PBC replicas within the plane. The size of the modelling volume was fixed to be 242×242×50 nm^3. Dashed line is an asymptote $y_0 = 0.73$ for remanence.

this approach led to a greater statistical scattering of the obtained results in comparison with ones for square modelling area, but mean values were close to each other.

At the first step, for an intermediate size of the modelling area of 242 nm, the dependencies of remanence and total energy density on the number of PBC replicas were obtained (Fig. 3). In general, the number of replicas indicates how many copies on each side of the simulation volume are added to calculate interaction fields. A continuous magnetic film should have infinite number of them that is not practically attainable. Thus, it should be a sufficiently large number but reasonable. It can be seen in Figure 3 that both total energy density and remanence are reaching constant values with an increase in the number of replicas. These results were accurately approximated by the sum of two exponents: $y = y_0 + A_1 e^{-x/t_1} + A_2 e^{-x/t_2}$. Hence, y_0 was an asymptotic value that was of 0.730 for the reduced remanence. 18 PBC replicas were chosen for further calculations, since at this number remanence was of 0.724 and its relative error was just of 0.8%. For comparison, 3 replicas gave a more significant error of about 8%.

Results of the main series of calculations for different sizes of modelling area are presented in Figures 4–6. In all cases weak stripe domains (Fig. 4a) were formed after gradual energy minimization starting from the saturated initial condition. The number of stripe domains varied depending on L in a discrete manner. That was because of periodic boundary conditions – only an integer number of stripe periods allowed to be inscribed in a given area. Thus, calculations showed that the same number of stripe periods remained over a certain range of sizes with narrowed or expanded width in respect to the width in the infinite film at the equilibrium. Only after a sufficient increase in size, it became profitable for such constrained system to add one more period of the stripe structure. This situation is well illustrated in Figure 4b where stripe domains are presented in cross-sections. A colorbar corresponds to the magnetization projection on Z-axis that is oriented normal to the film. Streamlines are plotted as tangent lines in the magnetization vector field revealing its features. It can be seen that several sizes of 206 nm, 242 nm, and 262 nm have the same number of stripes that become significantly wider with increasing L. An interesting situation is observed at 266 nm, where stripe cores are slightly shifted from the center in a periodic manner.

The main magnetic characteristics vary both within intervals of the same number of stripe periods and, in general, with an increase in the number of stripe periods (Fig. 5). Each interval of the same number of stripe periods is highlighted in the figure alternately in red and blue. For example, we noticed a characteristic feature in

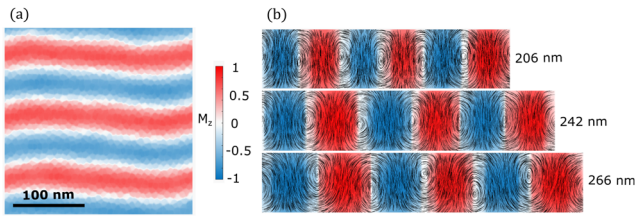

FIG. 4. Stripe domain patterns (a) top-view and (b) in cross-section for different sizes of the modelling area having 3 periods of stripes. The colors of the legend show the magnetization projection on Z-axis that is perpendicular to the film.

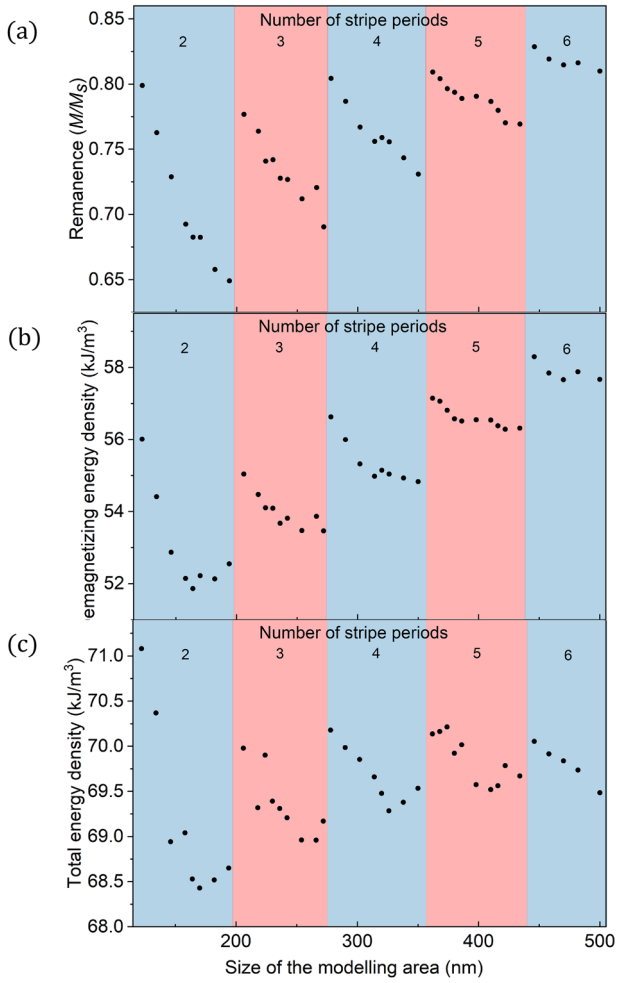

FIG. 5. Dependencies of the reduced remanence (a) demagnetizing energy density (b) and total energy density (c) of the columnar LaCo film on the lateral size of the modelling area. Intervals with the same number of stripe periods are alternately filled in red and blue.

the behavior of the remanence dependence: with an increase in the number of stripe periods, the spread in the magnetization values decreases, while there is a general trend towards an increase in remanence values. It can be assumed that the value gradually reaches a constant level, which lies slightly above the obtained data.

Dependence of stripe width on the size of the modelling area is shown in Figure 6. Again, there is a significant variation on size of modelling area. Let us note that both upper and lower limits of each interval with the same number of stripes tend to the asymptotic value. This trend was described well by the following exponential law $y = y_0 + A_1 e^{-x/t_1}$ (red dash lines) that gives an estimation of the equilibrium stripe width of 39.5 nm (black dash line). This width can be compared with an experimental one of 90 nm that was estimated from magnetic force microscopy of $La_{17}Co_{83}$ film at room temperature. There is a reasonable in order-of-magnitude agreement between these values. Their discrepancy can be caused by several reasons. First, the experimental width was obtained for the thinnest

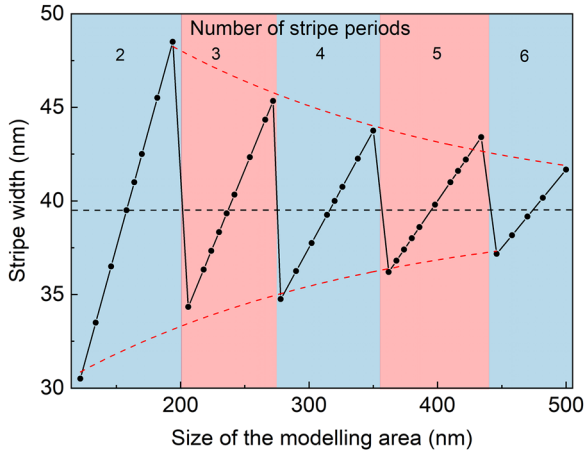

FIG. 6. Dependence of stripe width on the size of the modelling area. Intervals with the same number of stripe periods are alternately filled in red and blue.

LaCo film of 100 nm that was available for us. This thickness was twice as big as those in modelling, and the larger the thickness – the bigger the stripe width. Second, a slight difference in the nominal composition as well as nonoptimal matrix/columns composition ratio chosen for modelling also can yield the width variation. Further development of this work will be focused on achievement of better quantitative agreement between experiment and numeric data and optimization of the micromagnetic model. It will allow us to quantify structure-induced perpendicular magnetic anisotropy and even separate different sources of magnetic anisotropy if there are several of those in real films.

IV. CONCLUSION

In conclusion, we presented the micromagnetic model of thin magnetic films with columnar microstructure based on LaCo films. We showed that such nonuniform structure led to the formation of weak stripe domain pattern without perpendicular magnetic anisotropy when the main magnetic and microstructural parameters inherent in the model were taken from experimental data. We demonstrated that finite size of the modelling area and number of replicas of periodic boundary conditions significantly influenced on width of stripe domains, remanence and total magnetic energy density. This should be taken into account for modelling the objects with macroscopic domain structure. As a result, the optimal number of replicas was chosen to get an error of actual values of less than 1%. Also we estimated equilibrium width of stripe domains and remanence by extrapolating obtained dependencies on infinite magnetic film. Therefore, based on the parameters of our micromagnetic model, the estimated stripe domain width is 39.5 nm and the value of remanent magnetization related to saturation magnetization lies slightly above 0.8.

ACKNOWLEDGMENTS

This work was supported by Russian Science Foundation, project No. 19-72-00141.

DATA AVAILABILITY

The data that support the findings of this study are available from the corresponding author upon reasonable request.

REFERENCES

[1] X. Yu, M. Mostovoy *et al.*, PNAS **109**, 8856 (2012).
[2] A. Hubert and R. Schäfer, *Magnetic Domains: The Analysis of Magnetic Microstructures* (Springer, Berlin, 2009).
[3] C. Kittel, Phys. Rev. **70**, 965 (1946).
[4] N. Saito, H. Fujiwara, and Y. Sugita, J. Phys. Soc. Japan **19**, 1116 (1964).
[5] T. H. Johansen, A. V. Pan, and Y. M. Galperin, Phys. Rev. B **87**, 060402 (2013).
[6] Y. Yafet and E. M. Gyorgy, Phys. Rev. B **38**, 9145 (1988).
[7] F. Virot *et al.*, J. Phys. D: Appl. Phys. **45**, 405003 (2012).
[8] M. W. Muller, Phys. Rev. **122**, 1485 (1961).
[9] G. van der Laan *et al.*, Superlatices and Microstructures **34**, 107 (2003).
[10] K.-W. Moon *et al.*, Phys. Rev. Appl. **12**, 034030 (2019).
[11] R. Ferre, Computational Materials Science **10**, 205 (1998).
[12] K. Chesnel *et al.*, Phys. Rev. B **98**, 224404 (2018).
[13] J. McCord *et al.*, J. Appl. Phys. **113**, 073903 (2013).
[14] F. Valdes-Bango *et al.*, New J. Phys. **20**, 113007 (2018).
[15] A. Talapatra, J. Arout Chelvane, and J. Mohanty, J. Magn. Magn. Mat. **489**, 165469 (2019).
[16] B. Pianciola *et al.*, Phys. Rev. B **102**, 054438 (2020).
[17] A. Stellhorn *et al.*, J. Magn. Magn. Mat. **476**, 483 (2019).
[18] J. Brandenburg *et al.*, Phys. Rev. B **79**, 054429 (2009).
[19] I. Lemesh, F. Büttner, and G. S. D. Beach, Phys. Rev. B **95**, 174423 (2017).
[20] P. Agrawal *et al.*, Phys. Rev. B **100**, 104430 (2019).
[21] D. Mergel *et al.*, Phys. Rev. B **47**(2), 882 (1993).
[22] Y. Suzuki *et al.*, IEEE Trans. Magn. **23**, 2275 (1987).
[23] H. J. Leamy *et al.*, J. Phys. D: Appl. Phys. **10**, L95 (1977).
[24] *Handbook of Magnetic Materials*, Magnetic amorphous alloys by Hansen P, Vol. 6, edited by K. Buschow (Elsevier, 1991).
[25] A. Vansteenkiste *et al.*, AIP Adv. **4**, 107133 (2014).
[26] S. Uchiyama, Mater. Chem. Phys. **42**, 38 (1995).
[27] K. Shiba *et al.*, IEEE Trans. Magn. **22**, 1104 (1986).
[28] V. O. Vas'kovskiy *et al.*, Physics of the Solid State **57**, 1142 (2015).
[29] V. Jaccarino and L. R. Walker, Phys. Rev. Lett. **15**, 258 (1965).
[30] R. Moreno *et al.*, Phys. Rev. B **94**, 104433 (2016).